RESEARCH ARTICLE

Corrosion inhibition behavior of chalcone oxime derivatives on carbon steel in 0.5 M H$_2$SO$_4$

A. Thoume[1,2] · F. Benhiba[3] · A. Elmakssoudi[2] · D. Benmessaoud Left[1] · N. Benzbiria[1] · I. Warad[4] · M. Dakir[2] · M. Azzi[1] ·
M. Zertoubi[1] · A. Zarrouk[5]

Abstract

In this work the adsorption and corrosion inhibition conduct of chalcone oxime derivatives on carbon steel in 0.5 M sulfuric acid solution at various temperatures (293, 303, 313, and 323 K) were investigated through weight loss measurements, potentiodynamic polarization, and electrochemical impedance spectroscopy. Results reveal that CO–H and CO–OMe exhibit an excellent inhibition efficiency of 95 and 96% at a concentration of 4.48×10^{-4} M and 293 K, respectively. The compounds are classified as mixed type inhibitors. Moreover, the influence of temperature and the activation parameters disclose that CO–H and CO–OMe are chemisorbed on the carbon steel surface. The adsorption of CO–H and CO–OMe follows Langmuir isotherm. The surface morphology was evaluated using scanning electron microscopy (SEM) and the adsorption behavior was analyzed by UV–visible. MD simulation data show good agreement with experimental results.

✉ A. Zarrouk
  azarrouk@gmail.com

1   Laboratoire Interface Matériaux Environnement (LIME),
    Faculté des Sciences Ain Chock, Université Hassan II de
    Casablanca, B.P 5366, Casablanca, Morocco

2   Laboratoire de Synthèse Organique, Extraction et
    Valorisation (LSOEV), Faculté des Sciences Ain Chock,
    Université Hassan II de Casablanca, B.P 5366, Casablanca,
    Morocco

3   Laboratory of Advanced Materials and Process Engineering,
    Faculty of Sciences, Ibn Tofail University, B.P 242,
    14000 Kenitra, Morocco

4   Department of Chemistry and Earth Sciences, Qatar
    University, P.O. Box 2713, Doha, Qatar

5   Laboratory of Materials, Nanotechnology and Environment,
    Faculty of Sciences, Mohammed V University in Rabat,
    Av. Ibn Battouta, P.O. Box, 1014 Agdal, Rabat, Morocco

Graphic abstract
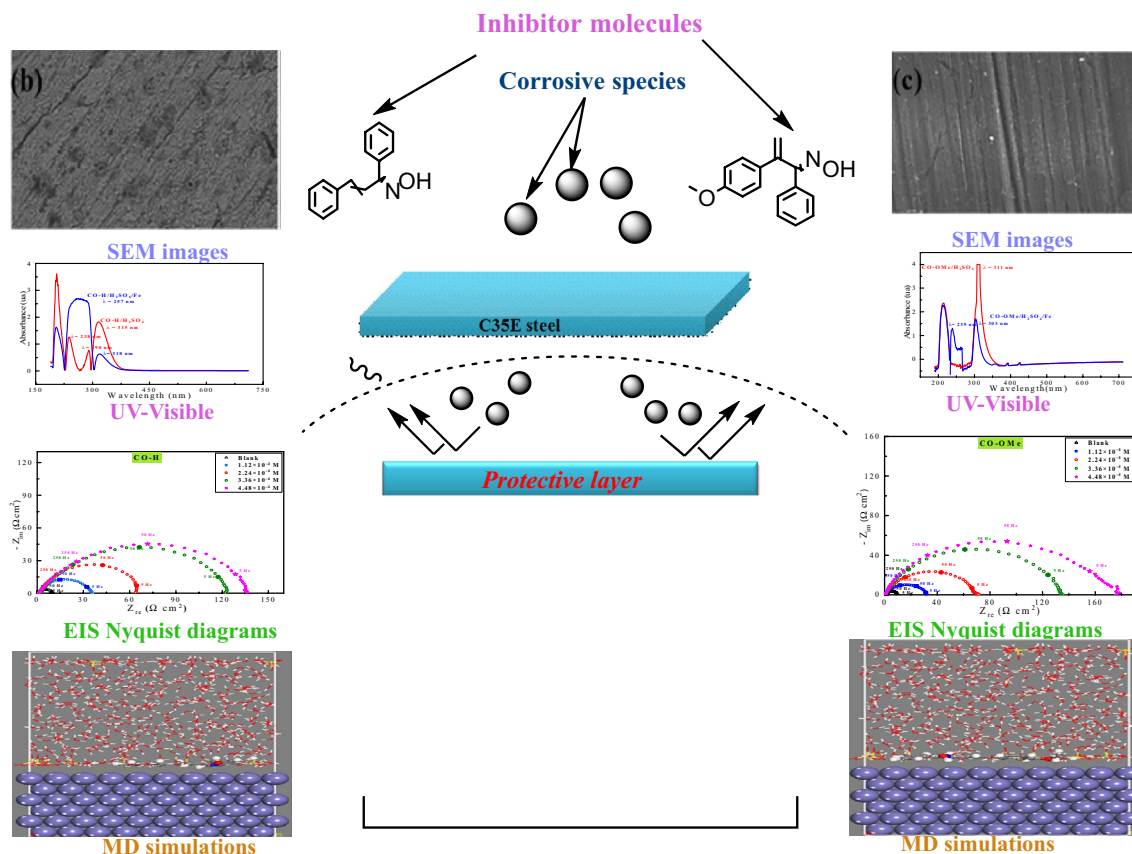
Keywords Chalcone oxime derivatives · Carbon steel corrosion · Langmuir · SEM/UV–visible · DFT/MD

1 Introduction

Steel has a favorable role owing to its superior technical characteristics. Nevertheless, it has the major drawback of possessing a fairly strong reactivity with the surrounding environment, which contributes more or less to their demise [1–3].Metal corrosion is a phenomenon in which metals and alloys tend to return to their original state of oxide, sulfide, carbonate, or any other salt that is more stable under the influence of chemical reagents or environmental agents [4, 5]. Petroleum corrosion is certainly much more common than elsewhere, considering the complexity of the conditions faced and the manufacturing situations in which prevention is practiced [6, 7]. Petroleum sites are the key victims of corrosion phenomena, particularly when utilizing acids that are frequently used in this industry, particular H_2SO_4 and HCl, in steel pickling, chemical washing, and boiler decaling [8–11]. Organic inhibitors, whose mode of action usually comes from their adsorption on the metal surface, are more commonly used

to solve this unfavorable tendency owing to their excellent biodegradability, easy availability, and non-toxic nature [12, 13]. Such compounds must fulfill other requirements: prevent the metal dissolution, slow the acid action, and remain stable at low concentrations [14–17].Successful organic inhibitors usually have in their structure either N, S, or O atoms and π-electrons in triple or conjugate double bonds [18–20].

Chalcone oxime has been used as selective retinoid receptor agonists RAR_γ, and tyrosinase inhibitors, and also applied to synthesize isoxazolines and isoxazoles, both of which are heterocycles very useful in organic and medicinal chemistry [21, 22]. Until now there is no research on the usage of chalcone oxime as a corrosion inhibitor, as well the cheap and straightforward synthesis of the product. Thus, in this situation, the investigation seems to be a significant study.

In this paper, chalcone was synthesized by the Claisen–Schmidt reaction and chalcone oxime derivatives via the condensation of chalcone and hydroxylamine
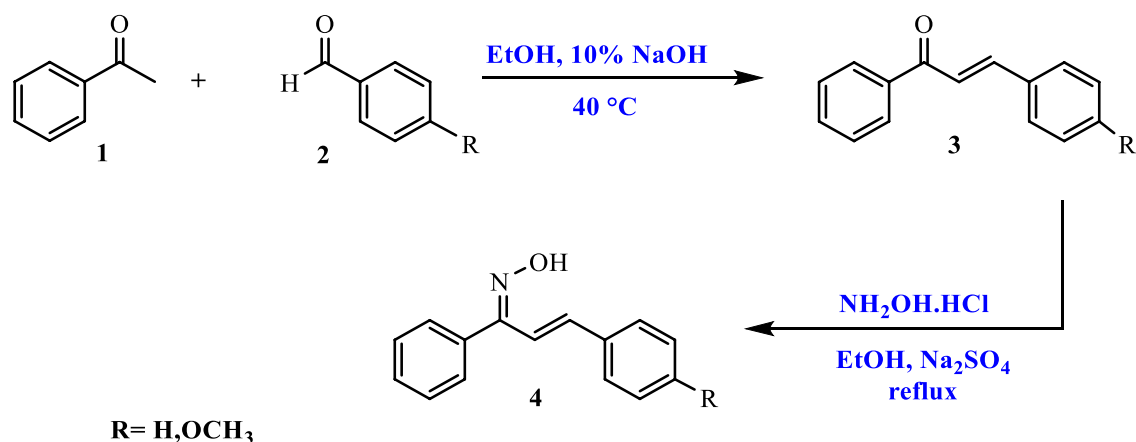
Scheme 1 Synthesis of the chalcone **3** and chalcone oxime **4**

hydrochloride (Scheme 1). The compounds inhibitory effect was inspected against the corrosion of carbon steel in 0.5 M H_2SO_4 solution at different temperatures (293–323 K). Various chemical and electrochemical techniques were used in this perspective. The surface morphology was examined using scanning electron microscopy to reveal the nature of the protective layer developed on carbon steel substrate. UV–visible technique was used to understand the adsorption action of the synthesized inhibitors over the carbon steel surface. To gain basic findings about interactions and surface adsorption of CO–H and CO–OMe, molecular dynamics (MD) simulation simulations were applied.

2 Materials and measurements

2.1 Preparation of chalcone 3 and chalcone oxime 4

- **Synthesis of chalcone**

In a round bottom flask (50 mL), placed in an ice bath, 20 mL of EtOH, 10 mmol of acetophenone **1** (11 mmol) of benzaldehyde derivatives **2** and 15 mL of 10% NaOH solution were added. Then kept on magnetic stirring at 40 °C for 4 h. The mixture was cooled slowly and left in freezer for 48 h and filtered under vacuum. The crude product was recrystallized from ethanol [23].

- **Synthesis of chalcone oxime**

A mixture of chalcone derivatives **3** (1 mmol), hydroxylamine hydrochloride (3 mmol), potassium carbonate (1 mmol), and anhydrous sodium sulfate (1.5 mmol) was refluxed in ethyl acetate (15 mL). After the reaction

completion, the mixture was filtered, and the solvent was evaporated under reduced pressure. Then distilled water (15 mL) and dichloromethane (15 mL × 3) were added to extract organic compounds. The organic extracts were combined, dried over anhydrous $MgSO_4$, filtered, and concentrated under reduced pressure. The crude mixture was obtained and purified by silica gel column chromatography eluted with a mixture of *n*-hexane–EtOAC (80/20, v/v) to afford pure product **4** [24].

2.2 Physical and spectroscopic data for chalcone oxime

1,3-diphenylprop-2-en-1-one oxime (CO–H); white solid, yield: 93%; mp 90–91 °C; ^{1}H NMR (300 Hz, $CDCl_3$): δ (ppm) 11.29 (s, 1H, OH), 7.78–7.56 (m, 4H), 7.46–7.31 (m, 6H), 7.29–6.38 (m, 2H). ^{13}C NMR (75 Hz, $CDCl_3$): δ (ppm) 157.74 (C=N); 139.76 (CH–C_{Ar}), 137.04 (C_{Ar}); 136.19 (Cq–CH=CH); 134.79 (Cq–C=N); 129.25–125.74 (C_{Ar}); 117.15 (CH=CH–Cq). IR (KBr) cm^{-1}: 3590 (OH); 2985 (CH); 1620 (C=N); 1514 (C=C); 945 (N–O).

  4-methoxyphenyl-1-phenylprop-2-en-1-one oxime (CO–OMe); white solid, yield: 88%; mp117–118 °C ^{1}H NMR (300 MHz, $CDCl_3$):δppm: 10.98 (s, 1H), 7.61–7.40 (m, 8H), 7.30–7.11 (m, 2H), 6.95–6.85 (m, 2H), 3.80 (s, 3H).^{13}C NMR (75 MHz, $CDCl_3$):δppm: 161.33 (Cq–O) 154.07 (C=N);136.29 (CH–C_{Ar}); 131.57 (Cq–CN), 130.85 (Cq–CH=CH); 128.62 (C_{Ar}); 128.60 (C_{Ar}); 127.24 (C_{Ar}); 123.18 (CH–CN); 114.28 (C_{Ar}); 55.31 (C–O).IR (KBr) cm^{-1}: 3600 (OH); 2995 (CH); 1640 (C=N); 1520 (C=C); 1310 (Ar–OMe).

2.3 Materials

The chemical composition of carbon steel operated as working electrode in this study is enclosed in Table 1. The

Table 1 Chemical composition of carbon steel C38

Element	C	Si	Mn	S	Cr + Ni + Mo	Fe
%wt	0.35–0.39	≤ 0.400	0.50–0.80	0.015–0.035	≤ 0.63	Remainder

corrosive solution (0.5 M H_2SO_4) was prepared by diluting an analytical reagent grade 98% H_2SO_4 with distilled water. In the meanwhile, various concentration gradients of chalcone oxime derivatives (1.12×10^{-4}, 2.24×10^{-4}, 3.36×10^{-4}, 4.48×10^{-4} M) at temperatures of 293 K were prepared to assess inhibition efficiency. Before each test, the electrode was polished by empery paper (200, 600, 800, and 1200), then washed with distilled water, acetone and dried.

2.4 Weight loss measurements

Weight loss was accomplished by exposing carbon steel specimens to 100 mL of 0.5 M H_2SO_4 solution for 6 h with differing chalcone oxime derivatives concentrations at 293 K. The surface of specimens (1 cm × 1 cm × 0.3 cm) underwent polishing pre-treatment prior to each trial. Afterward, carbon steel was washed by hot ethanol, distilled water, and acetone to remove all organic and inorganic matter, and then the samples were weighed. The corrosion rates (ν) were computed according to the following equation [25]:

$$\nu = \frac{\Delta W}{S \times t}, \tag{1}$$

$$\eta_W(\%) = \frac{\nu^0 - \nu}{\nu^0} \times 100, \tag{2}$$

where ΔW denotes the average weight loss, S represents the sample surface area (cm^2), t stands for the immersion time (h), ν^0 and ν designate the values of corrosion rate (mg cm^{-2} h^{-1}) in uninhibited and inhibited media, respectively.

2.5 Electrochemical measurements

In this study, the electrochemical measurements in this study were performed using PGZ301 electrochemical workstation with a classical three-electrode system: Pt as the counter electrode, a saturated calomel reference electrode (SCE), and carbon steel as a working electrode (0.282 cm^2). The carbon steel was maintained immersed in the corrosive medium until the open-circuit potential (OCP) was stabilized (40 min) before the electrochemical measurements. The potentiodynamic polarization (PDP) curves were plotted by a scan rate of 0.5 mV s^{-1} and the range of OCP ± 200 mV. The electrochemical impedance spectroscopy (EIS) was recorded at various frequencies between 100 kHz and 10 mHz in the OCP with an amplitude of 10 mV. The inhibition efficiency

(η) was estimated using both techniques PDP and EIS as following [26, 27]:

$$\eta_P(\%) = \frac{i_{corr}^0 - i_{corr}}{i_{corr}^0} \times 100, \tag{3}$$

i_{corr}^0 and i_{corr} denote the corrosion current densities values in absence and presence of the inhibitory molecule, respectively.

$$\eta_{EIS}(\%) = \frac{R_p^i - R_p^b}{R_p^i} \times 100, \tag{4}$$

where R_p^b and R_p^i are polarization resistances obtained in the blank and the inhibited solutions, respectively.

The surface coverage, θ is expressed as:

$$\theta = \frac{\eta_P(\%)}{100}, \tag{5}$$

η_P is the inhibitory efficiency determined by PDP.

2.6 Scanning electron microscopic measurement (SEM) and electrolyte analysis

The surface of carbon steel was polished with abrasive papers of different grades (200–1200) and sprayed with water and acetone, then the carbon steel was immersed for 6 h in 0.5 M H_2SO_4 with and without adding 4.48×10^{-4} M of synthesized inhibitory molecules. The specimens were extracted from the study solution and rinsed with distilled water and dried. The SEM images were obtained on an SEM FEI FEG 450. Weight reduction testing electrolytes are subject to an evaluation by means of UV mini-1240/UV–VIS Spectrophotometer with a view to confirming the iron-inhibitor complex formation that could happen upon dipping steel in a sulfuric acid electrolyte comprising inhibitor molecules.

2.7 Molecular dynamics (MD) simulation details

The adsorbed inhibitors CO and CO-NO$_2$ neutral and unnatural forms on the metal surface was established using the MD simulation using Forcite module implemented in Materials Studio 8.0 software [28, 29]. The study of these interactions of the molecules with the Fe (1 1 0) surfaces was carried out from a simulation box (22.34 × 22.341 × 35.13 Å^3) with periodic boundary conditions. The Fe (110) surface was presented with a 6-couche slab model in each layer representing a (9 × 9) unit cell. The constructed simulation box is

emptied by 20.13 Å^3. This vacuum is occupied by 500H$_2$O, 10H$_3$O$^+$, 5 SO_4^{2-} and the inhibitory molecule. The temperature of the simulated system of 293 K was controlled by the Andersen thermostat, NVT ensemble, with a simulation time of 400 ps, and a time step of 1.0 fs, all under the COMPASS force field [30].

3 Results and discussion
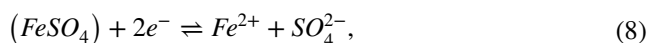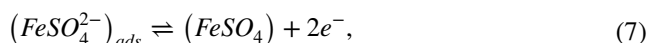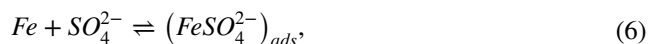
3.1 Weight loss measurements

The protection performance of CO–H and CO–OMe against carbon steel corrosion in 0.5 M H$_2$SO$_4$ at 293 K was calculated gravimetrically. Table 2 provides the values of corrosion rate and the inhibition activity. It can be noticed that the corrosion rate decreases with increasing CO–H and CO–OMe concentration. As a result, the inhibiting efficiency increases and reaches an inhibiting power of 93%

Table 2 Weight loss, corrosion rate, and inhibitory efficacy of CO–H and CO–OMe at different concentrations in 0.5 M H$_2$SO$_4$ medium
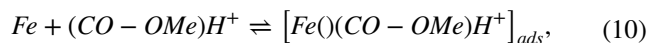
Medium	Concentration mol L^{-1}	ν mg cm^{-2} h^{-1}	η_W (%)
	Blank	2.880	–
CO–H	1.12×10^{-4}	1.200	58
	2.24×10^{-4}	0.566	80
	3.36×10^{-4}	0.366	87
	4.48×10^{-4}	0.216	93
CO–OMe	1.12×10^{-4}	0.866	70
	2.24×10^{-4}	0.350	88
	3.36×10^{-4}	0.233	92
	4.48×10^{-4}	0.150	95

and 95% in the presence of 4.48×10^{-4} M of CO–H and CO–OMe, respectively. The maximum protection efficiency for CO–OMe was due to the presence of electron donating methoxy group[31].This indicates that CO–H and CO–OMe covered the carbon steel surface through the adsorption and from it prevent the attack by the corrosive solution on the surface[32].The inhibition activity can be explained by the following equations[33]:
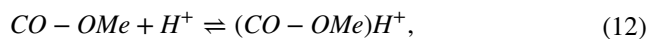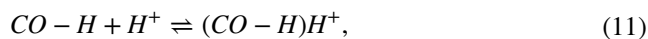
The iron dissolution reaction.

$$Fe + SO_4^{2-} \rightleftharpoons \left(FeSO_4^{2-}\right)_{ads}, \tag{6}$$

$$\left(FeSO_4^{2-}\right)_{ads} \rightleftharpoons \left(FeSO_4\right) + 2e^-, \tag{7}$$

$$\left(FeSO_4\right) + 2e^- \rightleftharpoons Fe^{2+} + SO_4^{2-}, \tag{8}$$

The inhibition mechanism

$$Fe + (CO - H)H^+ \rightleftharpoons \left[Fe()(CO - H)H^+\right]_{ads}, \tag{9}$$

$$Fe + (CO - OMe)H^+ \rightleftharpoons \left[Fe()(CO - OMe)H^+\right]_{ads}, \tag{10}$$

First of all, the protonation of CO

$$CO - H + H^+ \rightleftharpoons (CO - H)H^+, \tag{11}$$

$$CO - OMe + H^+ \rightleftharpoons (CO - OMe)H^+, \tag{12}$$

3.2 Potentiodynamic polarization (PDP)

PDP curves were plotted for carbon steel in H$_2$SO$_4$ environment in with and without different concentrations of CO–H and CO–OMe at 293 K. As seen in Fig. 1, the
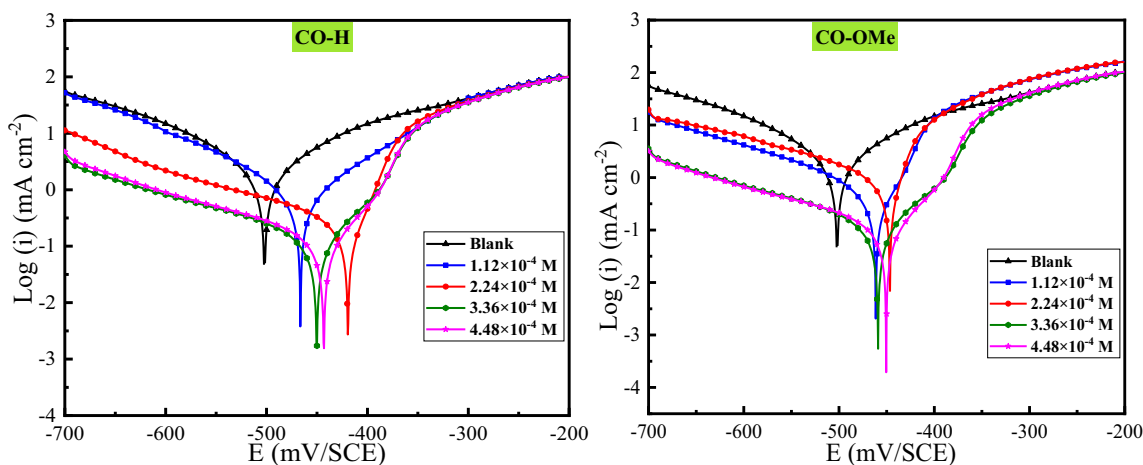

Fig. 1 PDP plots of carbon steel in 0.5 M H$_2$SO$_4$ solution containing CO–H and CO–OMe at 293 K

cathodic curves are in the form of a Tafel line, indicating that the H$^+$ reduction reaction on the steel surface takes place according to a pure activation mechanism [34]. As seen in Fig. 1, the addition of the CO–H and CO–OMe to the acid solution caused a significant reduction in the anodic and cathodic current densities. Concerning anodic polarization plots and especially in the higher concentrations for CO–H and CO–OMe inhibitors, it should be noted that one areas (1, and 2) are observed, which show the inhibited area, and uninhibited area, respectively. With augmenting anodic potentials, the anodic currents augmented with anodic Tafel slope β_{a1} in area 1. Next, for the rest of potential values, the desorption potential (E_{dsp}), the anodic currents rise sharply and dissolve at β_{a2} slope in area 2 and stabilized until the end forming a considerable flat. This flat can be ascribed to the shift of adsorption–desorption equilibrium toward the desorption of CO–H and CO–OMe molecules on the electrode surface [35].

Examination of Table 3 leads to the conclusion that the corrosion current densities in presence of the inhibitor are lower than those found in the blank test solution. It can be suggested that the inhibitors adsorb first on the carbon steel surface before acting by simple blocking through its active sites. Furthermore, on may notice that the corrosion potential gap is less than 85 mV for all concentrations and that both the anodic and cathodic partial currents are also reduced. These outcomes demonstrate the mixed nature with an anodic predominance of the inhibitors under study [36, 37], and show that the inhibitors CO–H and CO–OMe reduces both rates of the anodic dissolution of carbon steel and the reduction of H$^+$.

The fact that the Tafel slopes (β_a and β_c) do not present a defined behavior pattern with respect to the blank again support the claim that the adsorption process of CO–H and CO–OMe on carbon steel surface in 0.5 M H$_2$SO$_4$ solution is due to the blockage of active sites by the CO–H and CO–OMe compounds.

3.3 Electrochemical impedance spectroscopy

The study of electrochemical impedance diagrams at the corrosion potential for different concentrations was conducted to complete the understanding of the corrosion mechanisms of carbon steel and their prohibition in 0.5 M H$_2$SO$_4$ medium. From Fig. 2, one may see that the recorded impedance spectra consist of a unique capacitive loop that is not a perfect semicircle, which is attributed to the dispersion of the interfacial impedance frequency owed to the heterogeneity of the electrode surface [38, 39]. This heterogeneity may be the result of roughness, dislocations, impurities, adsorption, and can also be caused by the electrode's surface [40]. In general, this type of spectrum is assigned to a charge transfer mechanism taking place on a heterogeneous and irregular substrate [41].

Table 4 exhibits the data achieved following experimental results simulation with an equivalent circuit described in Fig. 2. In the 0.5 M H$_2$SO$_4$ alone and with 1.12×10^{-4}, 2.24×10^{-4}, 3.36×10^{-4}, and 4.48×10^{-4} M of CO–H and CO–OMe, the circuit consisted of an electrolyte resistance (R_e) in series with a polarization resistance (R_p) that is in parallel with a constant phase element (CPE), as illustrated in Fig. 2. The CPE is inserted to substitute a double layer capacitance (C_{dl}) to provide a more precise fit. The impedance of the CPE is established as [42]:

$$Z_{CPE} = A^{-1}(i\omega)^{-n}, \tag{13}$$

where A is the CPE modulus and n is a measure that reflects a deviation from the ideal behavior ranged from -1 to 1. Besides, the CPE is linked with the double layer capacitance (C_{dl}) by the next relationship [42]:

$$C_{dl} = \left(A^{1/n} R_P^{1-n/n} \right), \tag{14}$$

The chi-squared was utilized to appraise the precision of the fitting outcomes, the small chi-squared values (Table 4) acquired for all the outcomes show that the fitted

Table 3 Electrochemical descriptors estimated from PDP for carbon steel in 0.5 M H$_2$SO$_4$ with various concentrations of CO–H and CO–OMe at 293 K

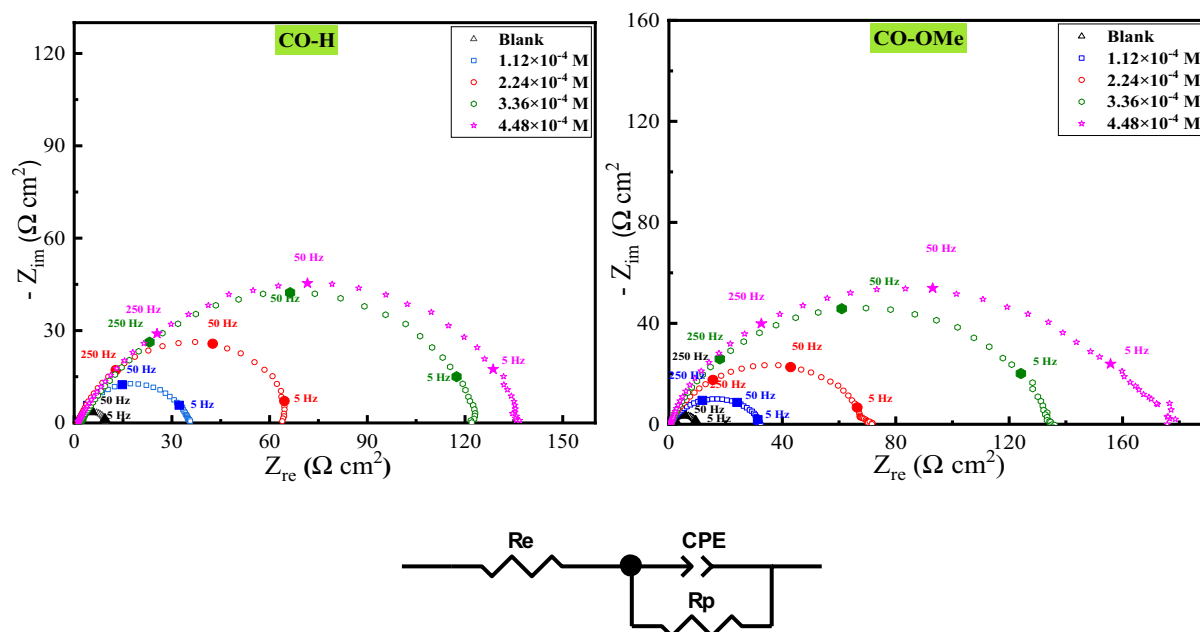| Medium	Concentration mol L^{-1}	$-E_{corr}$ mV$_{SCE}$	i_{corr} μA cm^{-2}	β_a mV dec^{-1}	$-\beta_c$ mV dec^{-1}	θ	η_p (%)
	Blank	501.4	2269.3	123	118.7	–	–
CO–H	1.12×10^{-4}	464.6	831.7	93.3	100.2	0.63	63
	2.24×10^{-4}	417.3	216.5	65.7	150.1	0.90	90
	3.36×10^{-4}	448.2	117.5	72.9	148.9	0.95	95
	4.48×10^{-4}	441.3	103.5	73.3	130.7	0.95	95
CO–OMe	1.12×10^{-4}	484.4	648.0	109.5	128.9	0.71	71
	2.24×10^{-4}	460.6	213.7	97.3	111.8	0.91	91
	3.36×10^{-4}	467.3	105.7	83.3	111.5	0.95	95
	4.48×10^{-4}	448.3	089.6	95.2	122.7	0.96	96

Fig. 2 Nyquist diagrams of carbon steel in 0.5 M H_2SO_4 solution containing CO–H and CO–OMe at 293 K and the employed circuit for fitting EIS spectra

Table 4 Electrochemical impedance descriptors of carbon steel in 0.5 M H_2SO_4 solution comprising varied concentrations of CO–H and CO–OMe at 293 K

Concentration (mol/L)	R_e (Ω cm^2)	R_p (Ω cm^2)	A ($\mu\Omega$ s^n cm^{-2})	n	C_{dl} (μF/cm^2)	η_{EIS} (%)	χ
CO–H							
Blank	1.18	8.3	826.4	0.853	350.2	–	0.002
1.12×10^{-4}	1.02	25.6	340.4	0.856	153.3	68	0.005
2.24×10^{-4}	1.64	65.2	113.6	0.859	50.8	87	0.001
3.36×10^{-4}	201	121.6	68.8	0.863	32.2	93	0.006
4.48×10^{-4}	1.78	137.3	57.1	0.869	27.5	94	0.006
CO–OMe							
1.12×10^{-4}	0.96	32.1	113.1	0.864	46.7	74	0.002
2.24×10^{-4}	0.92	68.8	71.9	0.869	32.3	88	0.004
3.36×10^{-4}	0.86	133.9	54.5	0.874	26.8	94	0.002
4.48×10^{-4}	1.07	176.2	37.1	0.884	19.2	95	0.006

results have a great concurrence with the experimental findings. The estimation of A for the reference electrolyte is larger than that of inhibited electrolyte; this proposes that the CO–H and CO–OMe molecules interacted with the electrode surface, thus reducing the destruction of exposed sites of the electrode. The highest R_p (137.3 Ω cm^2 for CO–H and 176.2 Ω cm^2 for CO–OMe) have been found at 0.448 mM. Indeed, increases in R_p values and the simultaneous reduction in C_{dl} as CO–H and CO–OMe concentration increased demonstrates the substitution of corrosive ions and water molecules from substrate surface with the inhibitor molecules, which rise the thickness of the electrical double layer, and decreases the local dielectric

constant, and it is a sign that CO–H and CO–OMe acted at the steel/acid interface [43]. However, the augments of the n value after the addition of CO–H and CO–OMe in 0.5 M H_2SO_4 electrolyte (0.856–0.884) relative to that achieved in reference electrolyte (0.853) can be interpreted as a certain diminution of the surface heterogeneity [44]. The corresponding values of η_{EIS}(%) for carbon steel in presence of CO–H are above that of CO–OMe and attaints 94% and 95% at 0.448 mM, respectively. These outcomes affirm once again that the synthesized compounds display potent inhibitive activity for carbon steel in 1/2 M H_2SO_4. It is worth noting that EIS trials confirm the superiority attached to the protection capacity of CO–H in relation

to CO–OMe, which is consistent with the data of weight reduction and PDP measurement.

3.4 Effect of temperature

Temperature can be considered as one of the factors that likely alter both the behavior of the steel in an aggressive environment and the nature of the interaction between the metal and the inhibitory molecules. In order to analyze the temperature effect on the inhibitory efficacy of the molecules under study, the polarization curves were plotted for carbon steel in 0.5 M H_2SO_4 with and without the addition of the CO–H and CO–OMe, in the temperature range going from 293 to 323 K (Fig. 3). The electrochemical descriptors derived from the polarization curves and the inhibiting efficiency are given in the Table 5. It can be noted that the increase in temperature causes an increment of i_{corr} value without and with the introduction of the inhibitors, while the values of the inhibiting efficiency are

almost constant in the temperature range studied (Table 5). This reflects strong adsorption of CO–H and CO–OMe (chemisorption) [45]. To understand the adsorption ability of the examined inhibitors, a detailed investigation was done using different activation and adsorption parameters.

Activation thermodynamic parameters were assessed using Arrhenius and transition state equations [46, 47]:

$$i_{corr} = A \times \exp\left(\frac{-E_a}{R \times T}\right), \tag{15}$$

$$i_{corr} = \frac{R \times T}{N \times h} \times \exp\left(\frac{-\Delta S_a}{R}\right) \exp\left(\frac{-\Delta H_a}{R \times T}\right), \tag{16}$$

where A represents a pre-exponential factor, ΔH_a designates the enthalpy, ΔS_a denotes the entropy of activation, T is the absolute temperature in Kelvin, h represents the Plank constant, N refers to the Avogadro number, and R is the molar
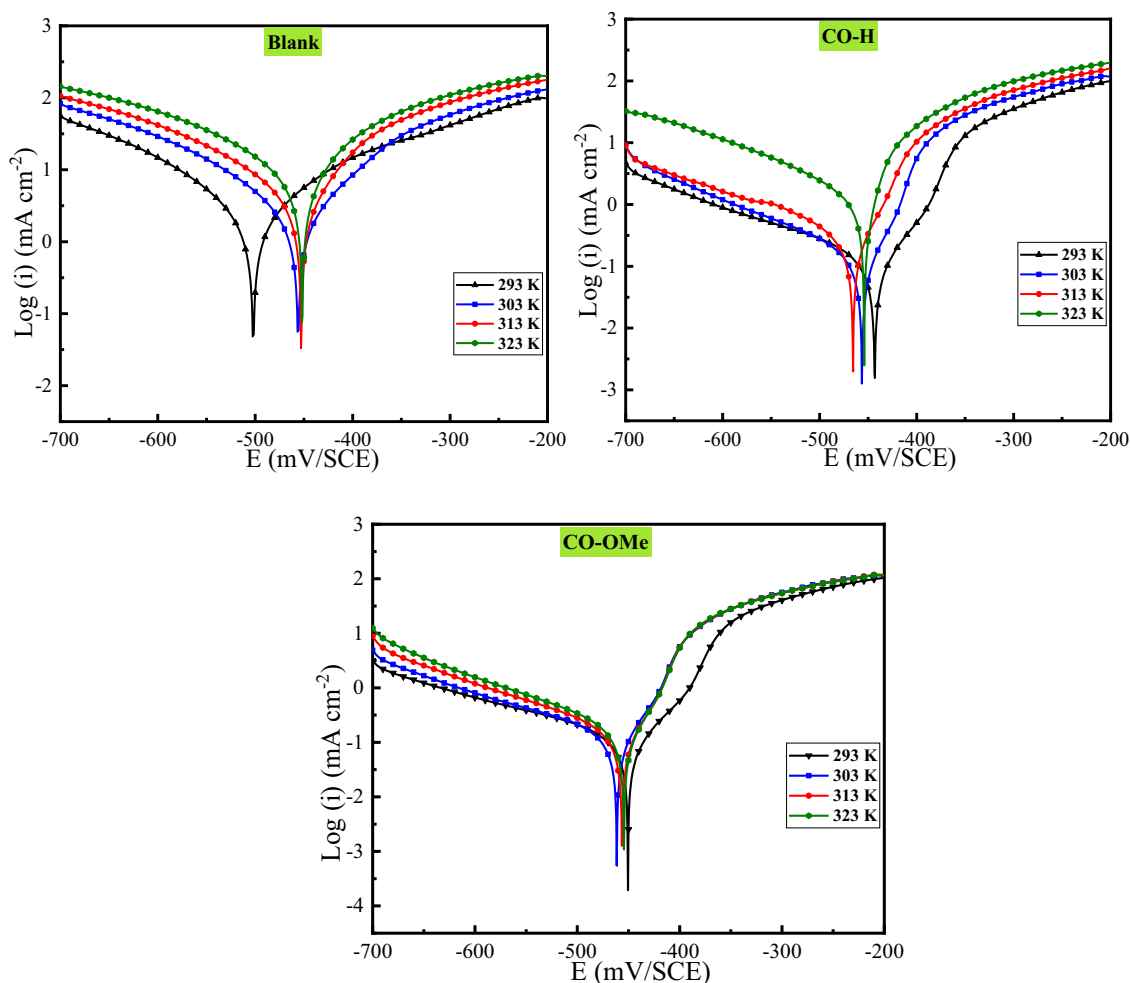

Fig. 3 PDP plots for carbon steel in the absence and presence of various concentrations of CO–H and CO–OMe at different temperature

Table 5 Electrochemical parameters derived from PDP plots for carbon steel in the absence and presence of various concentrations of CO–H and CO–OMe at different temperature

| Medium	Temperature (K)	$-E_{corr}$ mV$_{SCE}$	i_{corr} µA cm^{-2}	β_a mV dec^{-1}	$-\beta_c$ mV dec^{-1}	η_p (%)
Blank	293	501.4	2269.3	123.0	118.7	–
	303	454.1	4448.3	128.9	176.9	–
	313	450.9	6918.5	115.3	188.6	–
	323	449.9	11,315.9	130.9	193.9	–
CO–H	293	441.3	103.5	82.6	168.1	95
	303	454.3	154.2	78.4	162.2	97
	313	463.6	261.4	80.6	174.1	97
	323	452.2	452.1	87.5	183.6	96
CO–OMe	293	448.3	89.6	95.2	132.9	96
	303	507.0	121.5	103.5	102.4	97
	313	488.0	191.4	126.2	155.6	97
	323	487.6	309.2	135.1	179.3	97
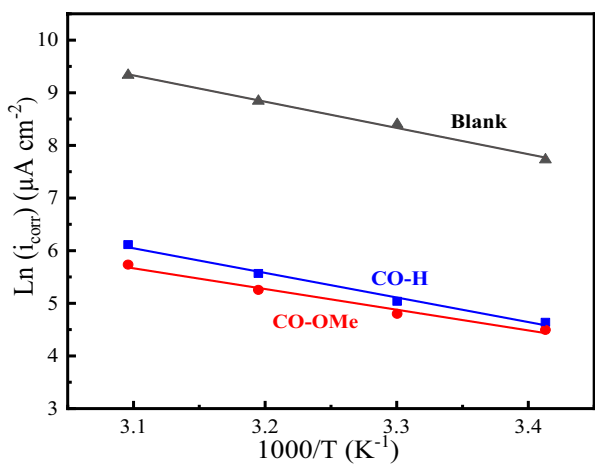
Fig. 4 Arrhenius plots for carbon steel in 0.5 M H$_2$SO$_4$ in the absence and the presence of CO–H and CO–OMe
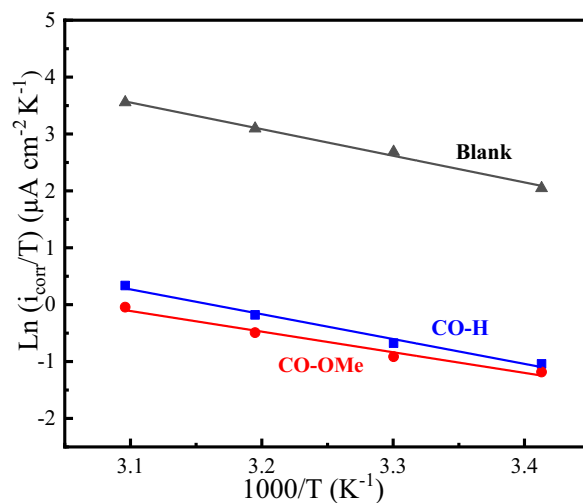

Fig. 5 Alternative Arrhenius plots for carbon steel in 0.5 M H$_2$SO$_4$ in the absence and the presence of CO–H and CO–OMe

Table 6 Activation parameters values of carbon steel in blank and with 4.48×10^{-4} M of CO–H and CO–OMe

Medium	E_a (kJ mol^{-1})	ΔH_a (kJ mol^{-1})	ΔS_a (J mol^{-1} K^{-1})
Blank	40.89	38.35	− 106.54
CO	38.40	35.86	− 141.51
CO–OMe	32.31	29.78	− 163.49

gas constant. Figure 4 shows the Arrhenius plots of Ln i$_{corr}$ versus 1/T.

It can be seen that the plot yields straight lines with almost unitary regression coefficients, which reveals that the corrosion mechanism obeys to the Arrhenius equation with a slope equal to ($-$E$_a$/R). The apparent activation energies (E$_a$) were computed and gathered in Table 6. The E$_a$ values of CO–H and CO–OMe were found lower than those of the blank test solution which reveals that the adsorption occurs upon the active centers having the greatest energies, whereas the corrosion mechanism takes place on the active centers possessing the lowest energies, and form it CO–H and CO–OMe are typically chemisorbed on the carbon steel surface [48]. From Fig. 5, ΔH_a and ΔS_a values were calculated and are listed in Table 6.

The positive values of ΔH_a confirm that the formation of activated complex is an endothermic process, while the negative values of ΔS_a suggest that the order takes place, through transformation from reactants to activate complex [49, 50].

3.5 Adsorption isotherm

The action of organic inhibitors occurs generally through adsorption onto the metallic surface. This adsorption can be considered as a quasi-replacement process betwixt the organic product in the aqueous phase $Org_{(aq)}$ and H_2O molecules following the reaction below [51]:

$$Org_{(S)} + xH_2O_{(ads)} \rightarrow Org_{(ads)} + xH_2O_{(S)}, \tag{17}$$
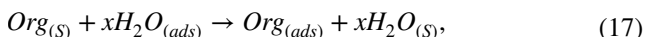
where x refers to the number of H_2O molecules displaced by the inhibitory molecules. The investigation of the adsorption type and the determination of the thermodynamic parameters characterizing this adsorption often enable to elucidate the action mode of these inhibitory compounds. To identify the adsorption type corresponding to the inspected inhibitors, diverse forms of isotherms were tested: Langmuir, Frumkin, and Temkin. It can be noticed that the Langmuir isotherm has the correlation nearly equal to the unity (Fig. 6), which is expressed by the subsequent equation [52]:

$$\frac{C}{\theta} = \frac{1}{K_{ads}} + C, \tag{18}$$

where θ represents the surface coverage, C refers to the inhibitor's concentration, and K_{ads} denotes the adsorption equilibrium constant. The high values of K_{ads} (K_{ads}(CO–H) $= 1.51 \times 10^4$ M^{-1} and K_{ads}(CO–OMe) $= 2.12 \times 10^4$ M^{-1}) are an indication of a stronger adsorption of CO–H and CO–OMe on the carbon steel surface [53, 54]. In a way to obtain a deeper insight of the CO adsorption mechanism, the standard adsorption free energy (ΔG°_{ads}) associated with K_{ads} were estimated by this equation [55]:

$$K_{ads} = \frac{1}{55.5} \times \exp\left(\frac{-\Delta G^{\circ}_{ads}}{R \times T}\right), \tag{19}$$

where 55.5 represents the water concentration in mol/L, R denotes the universal gas constant, and T refers to the absolute temperature. The negative value of ΔG°_{ads} indicates the stability of the double layer adsorbed on the metal surface [56]. According to literature, the values of ΔG°_{ads} near to -20 kJ/mol or more positive, corresponds to charged molecules/charged metal interaction (physical adsorption), whereas values close to -40 kJ/mol or more negative implies a charge transfer between the organic molecules and the metallic substrate (chemisorption) [57, 58]. The values of ΔG°_{ads} show that the studied inhibitors (ΔG°_{ads} (CO–H) $= -33.2$ kJ/mol and ΔG°_{ads}(CO–OMe) $= -34.3$ kJ/mol), is chemisorbed on the carbon steel surface and also uses the electrostatic interactions betwixt the charged molecules/charged metal interface, which points out to a mixed adsorption process [59].

3.6 Surface analysis

Scanning electron microscopy (SEM) was used to assess the morphology of the steel surface and confirm whether inhibition is owed to the development of an organic film on the surface. On one hand, the image of the electrode surface after an immersion time of 6 h at 293 K in 0.5 M H_2SO_4 (Fig. 7a), show that the dissolution of the metal makes the substrate very rough. While in the presence 4.48×10^{-4} M of CO–H or CO–OMe (Fig. 7a, c) the surface is covered with a platelet-shaped product reflecting the presence of an organic compound. From these observations, it seems that that the inhibition is owed to the development of an adherent and stable deposit that hinders the electrolyte's arrival to the steel surface [60, 61].

3.7 UV–visible spectroscopic studies

UV–visible spectroscopic measurements were conducted for 0.5 M H_2SO_4 solution in absence and presence of 4.48×10^{-4} M of either CO–H or CO–OMe before and after an immersion time of 48 h immersion of carbon steel at 293 K. The electronic absorption spectra (Fig. 8) of CO–H and CO–OMe before the steel immersion display a main visible band at 200, 238, 290, 315 nm, and 311,214 nm, respectively. The observed band can be attributed to π–$\pi \times$ transition related to aromatic ring and n–$\pi \times$ electronic transition from oxime groups. After 48 h of steel immersion, it can be seen that the UV–visible spectra of CO–H seem to change. In fact, there is a slight shift from 315 to 318 nm and disappear two bands at 238,290 nm with an appearance at 257 nm. For CO–OMe UV–visible spectra show a shift from 311 to
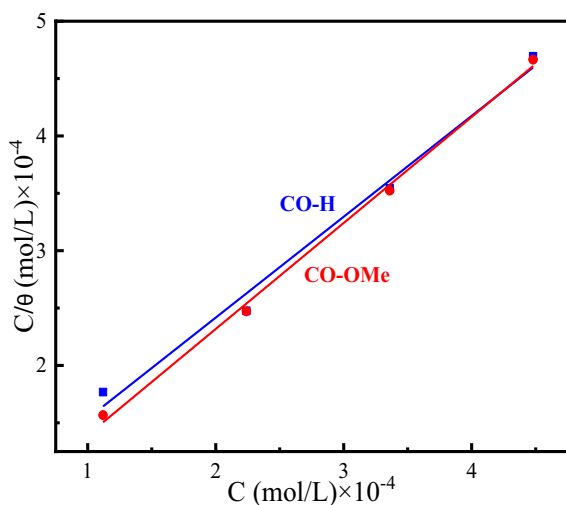

Fig. 6 Langmuir adsorption isotherm of CO–H and CO–OMe on carbon steel in 0.5 M H_2SO_4
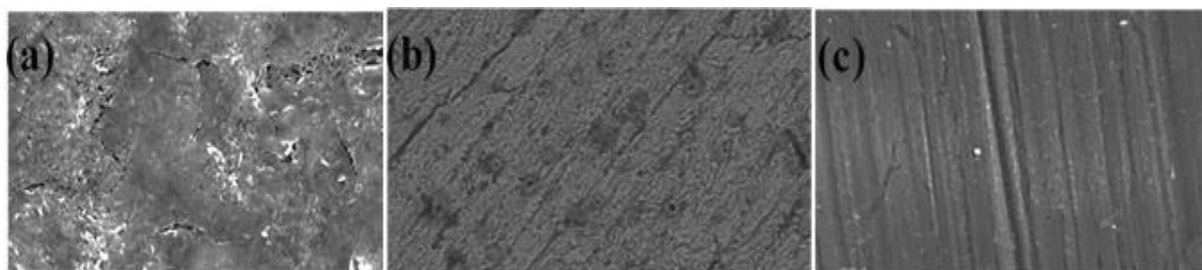
Fig. 7 Scanning electron micrographs of carbon steel samples at 293 K: **a** after 6 h immersion in 0.5 M H_2SO_4, **b** after 6 h immersion with 4.48×10^{-4} M of CO–H in 0.5 M H_2SO_4, **c** after 6 h immersion with 4.48×10^{-4} M of CO–OMe in 0.5 M H_2SO_4
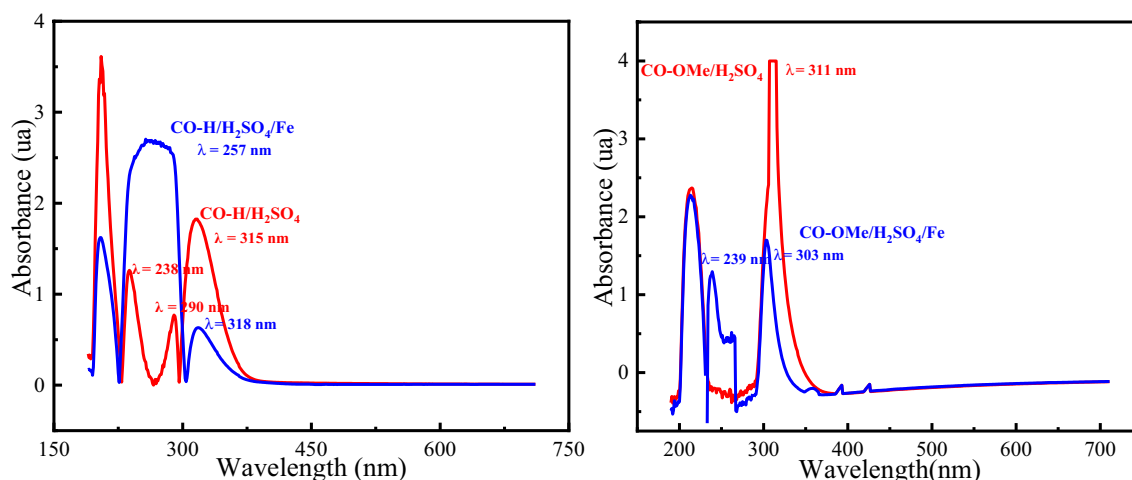

Fig. 8 UV–visible spectra of the carbon steel in the presence of CO before and after 48 h immersion in 0.5 M H_2SO_4

303 nm and an appearance band at 257 nm. These experimental findings may be assigned to the creation of a complex among Fe^{2+} and CO–H and/or CO–OMe in 0.5 M H_2SO_4 [62, 63].

3.8 MD simulation

In this last section, we have exploited molecular dynamics simulation as a very useful and efficient approach to clarify the reactivity or the action mode of the studied molecules in relation to the steel surface used in a sulfuric acid (H_2SO_4) environment [64–66]. Figures 9 and 10 give the preferred adsorption configuration of adsorbents in both neutral and protonated forms and their radial distribution functions (RDF) on the first well-ordered layer of iron. The configurations presented inform us about the adoption performance of each species on the simulated iron substrate. As visualized by each configuration (Figs. 9 and 10) that the compounds CO–H, CO–HH, CO–OMe, and CO–OMeH adsorb through all their skeletons onto the substrate, showing that these species favor the reduction of steel metal degradation of iron in H_2SO_4.

With respect to the overviews obtained from the RDF in Figs. 9 and 10, we can see that the values of the first peaks are lower than 3.5. These properties make it possible to reinforce the adsorption of the investigated inhibitor molecules on the surface of the metal; consequently, there is a reduction in the active sites on this area [67]. Additionally, protonation of CO–H, CO–H, and CO–OMe leads to the elongation of the studied bond lengths, which negatively influences on the rigidity of the adsorbed layer on the surface of the iron.

The interfacial interactions of species Co and CO–OMe no-charged and loaded forms with the Fe-surface were assessed using the interaction energy ($E_{interaction}$) [68]:

$$E_{\text{interaction}} = E_{total} - (E_{surface+solution} + E_{inhibitor}), \quad (18)$$

Based on the simulation data to calculate the interaction energy ($E_{interaction}$), the values of this descriptor are collected in Table 7. The negative value of $E_{interaction}$ confirms a large spontaneous adsorption of the selected molecules on the Fe (110) substrate [69–72]. Thus, neutral and protonated inhibitors tend to adsorb in the acid solution thermodynamically
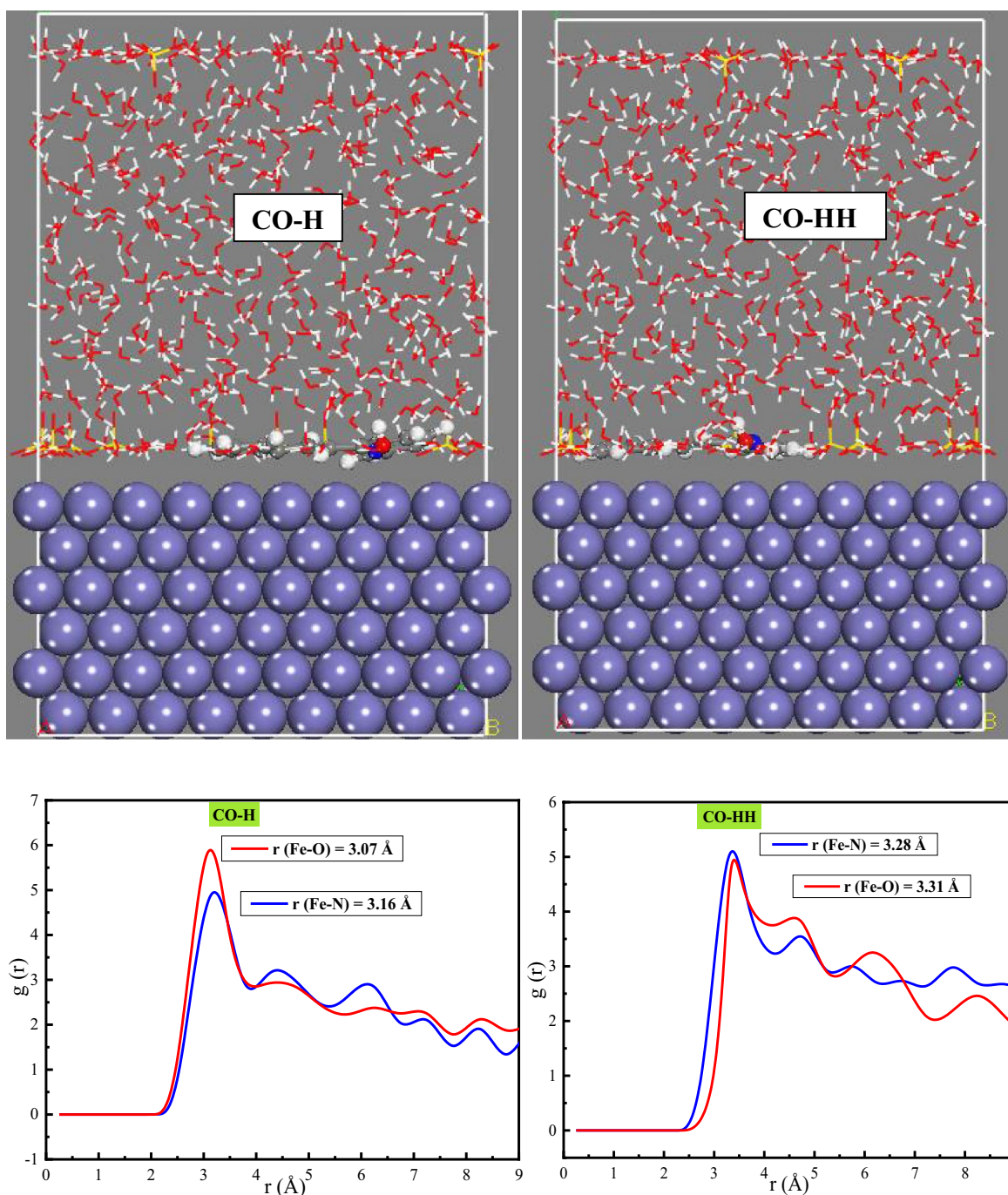
Fig. 9 MD snapshots and RDF of the preferred adsorption configuration of adsorbents in both CO–H and COHH on the first well-ordered layer of iron

on the Fe of the steel in question. The minimum value of CO–OMe/Fe (110) shows that this molecule reacts strongly with the iron surface. This data validates the results obtained by the experiments.

Based on the MD simulation data, the neutral and protonated forms of the studied molecules adsorb in parallel on the steel surface, which shows a strong adsorption of these

inhibitors. The nature of this adsorption can be chemical by the coordination bonds made between the electronic doublet of oxygen (O) of the tested inhibitors and the vacant orbitals found in the iron atoms (donation effect), the reverse effect (donation) allows the chemical adsorption to be reinforced. Physical adsorption occurs between the protonated nitrogen atom of the cationic forms (COHH
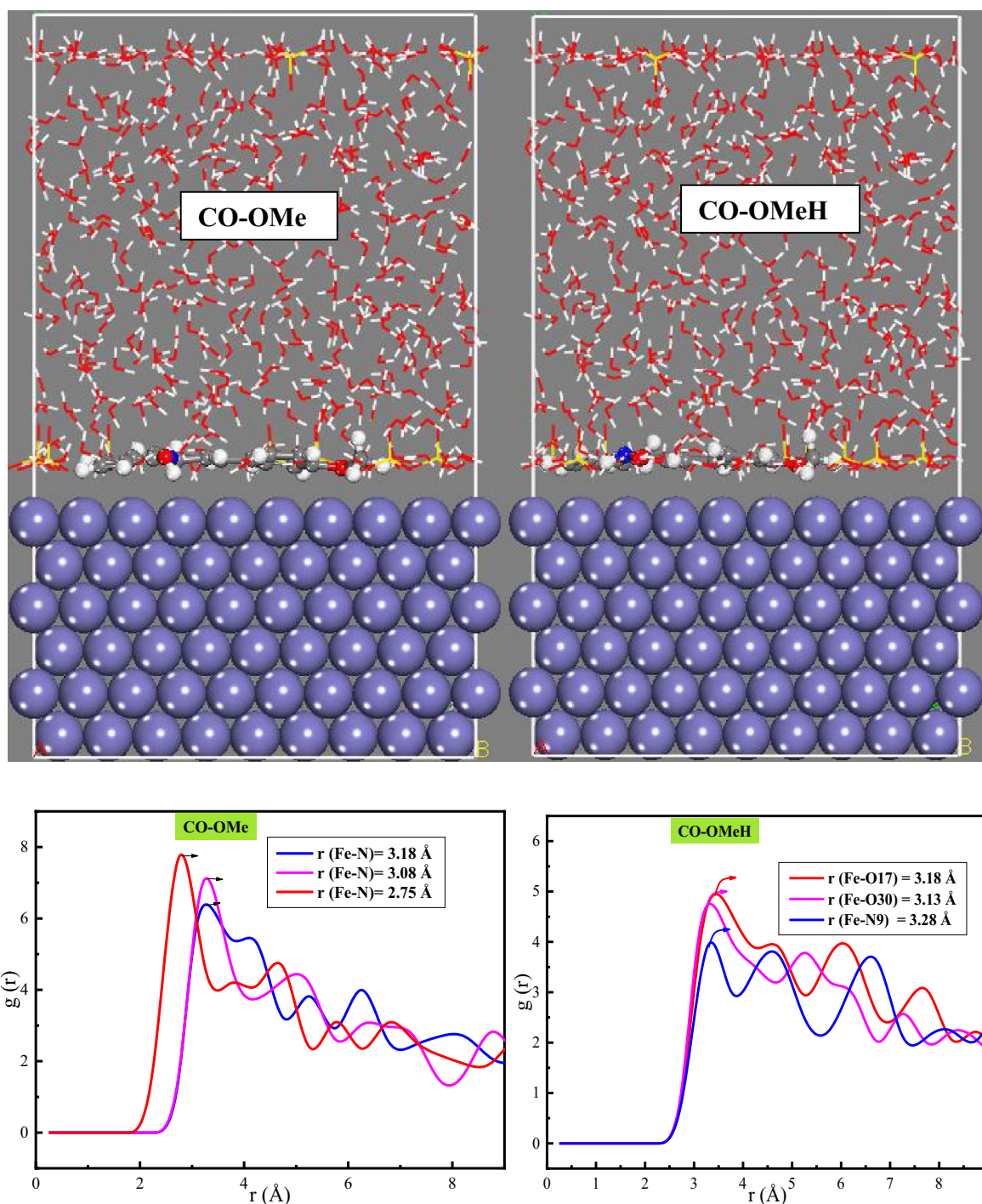
Fig. 10 MD snapshots and RDF of the preferred adsorption configuration of adsorbents in both CO–OMe and CO–OMeH on the first well-ordered layer of iron

and CO–OMeH) and the chlorine anions (Cl⁻) adsorbed on the iron surface. Therefore, if we assume that the inhibitor CO–OMe does not protonate in the acidic medium, in this case chemical adsorption will be in the majority which leads to a better inhibition against corrosion.

4 Conclusion

CO–H and CO–OMe were synthesized and characterized. Various techniques such as weight loss, PDP, and EIS were

Table 7 $E_{interaction}$ of systems inhibitors/Fe (110)

Systems (inhibitors/Fe(110))	$E_{interaction}$ (kJ/mol)
COH/Fe(110)	− 689.093
COHH/Fe(110)	− 672.941
CO–OMe/Fe(110)	− 741.863
CO–OMeH/Fe(110)	− 700.037

operated to evaluate the inhibitory efficacy on the carbon steel in 0.5 M H_2SO_4. Several conclusions are found and are summarized as follows:

- CO–OMe has slight advantage as a good inhibitory efficacy of carbon steel in 0.5 M sulfuric acid solution than CO-H and both acts as a mixed type.
- The temperature effect indicates the CO–H and CO–OMe is chemisorbed on the carbon steel surface.
- The adsorption of CO–H and CO–OMe on the carbon steel surface obeys Langmuir isotherms.
- The scanning electron microscopy (SEM) show the formation of a protective film on the surface of carbon steel.
- UV–visible spectra shown the formation of a complex between Fe^{2+} and CO–H and/or CO–OMe in 0.5 M H_2SO_4
- Molecular dynamics simulations reveal the strong interaction between the CO–H and CO–OMe and the iron surface.

References

1. Chung IM, Hemapriya V, Kim SH, Ponnusamy K, Arunadevi N, Chitra S, Prabakaran M, Gopiraman M (2021) Liriope platyphylla extract as a green inhibitor for mild steel corrosion in sulfuric acid medium. Chem Eng Commun 208(1):72–88
2. Elkholy AE, El-TaibHeakal F (2018) Electrochemical measurements and semi-empirical calculations for understanding adsorption of novel cationic Gemini surfactant on carbon steel in H_2SO_4 solution. J Mol Struct 1156:473–482
3. Barrahi M, Elhartiti H, El Mostaphi A, Chahboun N, Saadouni M, Salghi R, Zarrouk A, Ouhssine M (2019) Corrosion inhibition of mild steel by Fennel seeds (*Foeniculum vulgare* Mill) essential oil in 1 M hydrochloric acid solution. Int J Corros Scale Inhib 8(4):937–953
4. Abdel Nazeer A, Madkour M (2018) Potential use of smart coatings for corrosion protection of metals and alloys. J Mol Liq 253:11–22
5. Heusler KE, Landolt D, Trasatti S (1989) Electrochemical corrosion nomenclature. J Electroanal Chem Interfacial Electrochem 274:345–348
6. Soltani N, Tavakkoli N, Attaran A, Karimi B, Khayatkashani M (2020) Inhibitory effect of *Pistacia khinjuk* aerial part extract for carbon steel corrosion in sulfuric acid and hydrochloric acid solutions. Chem Pap 74:1799–1815
7. Chai C, Xu Y, Li D, Zhao X, Xu Y, Zhanga L, Wu Y (2019) Cysteamine modified polyaspartic acid as a new class of green

corrosion inhibitor for mild steel in sulfuric acid medium: synthesis, electrochemical, surface study and theoretical calculation. Prog Org Coat 129:159–170
8. Laabaissi T, Benhiba F, Rouifi Z, Missioui M, Ourrak K, Oudda H, Ramli Y, Warad I, Allali M, Zarrouk A (2019) New quinoxaline derivative as a green corrosion inhibitor for mild steel in mild acidic medium: Electrochemical and theoretical studies. Int J Corros Scale Inhib 8(2):241–256
9. Nabah R, Benhiba F, Ramli Y, Ouakki M, Cherkaoui M, Oudda H, Touir R, Warad I, Zarrouk A (2018) Corrosion inhibition study of 5, 5-diphenylimidazolidine-2, 4-dione for mild steel corrosion in 1 M HCl solution: experimental, theoretical computational and Monte Carlo simulations studies. Anal Bioanal Electrochem 10(10):1375–1398
10. Ma X, Dang R, Kang Y, Gong Y, Luo J, Zhang Y, Fu J, Li C, Ma Y (2020) Electrochemical studies of expired drug (formoterol) as oilfield corrosion inhibitor for mild steel in H_2SO_4 media. Int J Electrochem Sci 15:1964–1981
11. Zarrok H, Zarrouk A, Salghi R, Ramli Y, Hammouti B, Assouag M, Essassi EM, Oudda H, Taleb M (2012) 3,7-Dimethylquinoxalin-2-(1H)-one for inhibition of acid corrosion of carbon steel. J Chem Pharm Res 4(12):5048–5055
12. Hamdani I, El Ouariachi E, Mokhtari O, Salhi A, Chahboun N, El Mahi B, Bouyanzer A, Zarrouk A, Hammouti B, Costa J (2015) Chemical constituents and corrosion inhibition of mild steel by the essential oil of thymus algeriensis in 1.0 M hydrochloric acid solution. Der Pharm Chem 7(8):252–264
13. El-Rabiei MM, Nady H, Zaki EG, Negem M (2019) Theoretical and experimental investigation of the synergistic infuence of tricine and iodide ions on the corrosion control of carbon steel in sulfuric acid electrolyte. J Bio Tribo Corros 5:103. https://doi.org/10.1007/s40735-019-0298-5
14. Rbaa M, Galai M, Abousalem AS, Lakhrissi B, EbnTouhami M, Warad I, Zarrouk A (2020) Synthetic, spectroscopic characterization, empirical and theoretical investigations on the corrosion inhibition characteristics of mild steel in molar hydrochloric acid by three novel 8-hydroxyquinoline derivatives. Ionics 26:503–522
15. Fergachi O, Benhiba F, Rbaa M, Ouakki M, Galai M, Touir R, Lakhrissi B, Oudda H, Ebn Touhami M (2019) Corrosion inhibition of ordinary steel in 5.0 M HCl medium by benzimidazole derivatives: electrochemical, UV–visible spectrometry, and DFT calculations. J Bio Tribo Corros 5:21. https://doi.org/10.1007/s40735-018-0215-3
16. El Faydy M, Rbaa M, Lakhrissi L, Lakhrissi B, Warad I, Zarrouk A, Obot IB (2019) Corrosion protection of carbon steel by two newly synthesized benzimidazol-2-ones substituted 8-hydroxyquinoline derivatives in 1 M HCl: experimental and theoretical study. Surf Interfaces 14:222–237
17. Guo L, Tan J, Kaya S, Leng S, Li Q, Zhang F (2020) Multi-dimensional insights into the corrosion inhibition of 3,3- dithiodipropionic acid on Q235 steel in H_2SO_4 medium: a combined experimental and in silico investigation. J Colloid Interface Sci 570:116–124
18. Zarrouk A, Hammouti B, Zarrok H, Salghi R, Dafali A, Bazzi Lh, Bammou L, Al-Deyab SS (2012) Electrochemical impedance spectroscopy and weight loss study for new pyridazine derivative as inhibitor for copper in nitric acid. Der Pharm Chem 4(1):337–346
19. Zarrok H, Al Mamari K, Zarrouk A, Salghi R, Hammouti B, Al-Deyab SS, Essassi EM, Bentiss F, Oudda H (2012) Gravimetric and electrochemical evaluation of 1-allyl-1Hindole-2,3-dione of carbon steel corrosion in hydrochloric acid. Int J Electrochem Sci 7:10338–10357
20. Louadi YE, Abrigach F, Bouyanzer A, Touzani R, El Assyry A, Zarrouk A, Hammouti B (2017) Theoretical and experimental studies on the corrosion inhibition potentials of two tetrakis

pyrazole derivatives for mild steel in 10 M HCl. Port Electrochim Acta 35(3):159–178

21. Radhakrishnan S, Shimmon R, Conn C, Baker A (2015) Integrated kinetic studies and computational analysis on naphthyl chalcones as mushroom tyrosinase inhibitors. Bioorg Med Chem Lett 25(19):4085–4091

22. Xu X, Li J, Du C, Song Y (2011) Improved synthesis of 1,3-Diaryl-2-propen-1-one oxime in the presence of anhydrous sodium sulfate. Chin J Chem 29(12):2781–2784

23. Qian Y, Ma GY, Yang Y, Cheng K, Zheng QZ, Mao WJ, Shi L, Zhao J, Zhu HL (2010) Synthesis, molecular modeling and biological evaluation of dithiocarbamates as novel antitubulin agents. Bioorg Med Chem 18:4310–4316

24. Wang YT, Qina YJ, Zhang YL, LiY J, Rao B, Zhang YQ, Yang M, Jiang AQ, Qi JL, Zhu HL (2014) Synthesis, biological evaluation, and molecular docking studies of novel chalcone oxime derivatives as potential tubulin polymerization inhibitors. RSC Adv 4:32263–32275

25. Zarrok H, Zarrouk A, Salghi R, Oudda H, Hammouti B, Assouag M, Taleb M, EbnTouhami M, Bouachrine M, Boukhris S (2012) Gravimetricandquantumchemical studies of 1-[4-acetyl-2-(4-chlorophenyl)quinoxalin-1(4H)-yl]acetone as corrosion inhibitor for carbon steel in hydrochloric acid solution. J Chem Pharm Res 4(12):5056–5066

26. Tazouti A, Galai M, Touir R, EbnTouhami M, Zarrouk A, Ramli Y, Saraçoğlu M, Kaya S, Kandemirli F, Kaya C (2016) Experimental and theoretical studies for mild steel corrosion inhibition in 1.0 M HCl by three new quinoxalinone derivatives. J Mol Liq 221:815–832

27. Zarrouk A, Hammouti B, Dafali A, Zarrok H (2011) L-Cysteine methyl ester hydrochloride: a new corrosion inhibitor for copper in nitric acid. Der Pharma Chem 3(4):266–274

28. Echchihbi E, Nahlé A, Salim R, Benhiba F, Moussaif A, El-Hajjaji F, Oudda H, Guenbour A, Taleb M, Warad I, Zarrouk A (2020) Computational, MD simulation, SEM/EDX and experimental studies for understanding adsorption of benzimidazole derivatives as corrosion inhibitors in 10 M HCl solution. J Alloys Compd 844:155842

29. Accelrys (2016) Materials studio, revision 8.0. Accelrys Inc., San Diego

30. Andersen HC (1980) Molecular dynamics simulations at constant pressure and/or temperature. J Chem Phys 72:2384–2393

31. Benhiba F, Elaoufir Y, Belayachi M, Zarrok H, El Assyry A, Zarrouk A, Hammouti B, Ebenso EE, Guenbour A, Al Deyab SS, Oudda H (2014) Theoretical and experimental studies on the inhibition of 1,1'-(2-phenylquinoxaline 1,4-diyl)diethanone for the corrosion of carbon steel in 1.0 M HCl. Der Pharm Lett 6(4):306–318

32. Laamari MR, Benzakour J, Berrekhis F, Bakasse M, Villemin D (2012) Investigation of the effect of piperidin-1-yl-phosphonic acid on corrosion of iron in sulfuric acid. Arab J Chem 9(S2):S1218–S1224

33. Solmaz R, Mert ME, Kardaş G, Yazici B, Erbıl M (2008) Adsorption and corrosion inhibition effect of 1,1'-thiocarbonyldiimidazole on mild steel in H_2SO_4 solution and synergistic effect of iodide ion. Acta Phys Chim Sin 24:1185–1191

34. Derfouf H, Harek Y, Larabi L, Basirun WJ, Ladan M (2019) Corrosion inhibition activity of carbon steel in 1.0 M hydrochloric acid medium using hammada scoparia extract: gravimetric and electrochemical study. J Adhes Sci Technol 33(8):808–833

35. Li X, Xie X, Deng S, Du G (2014) Two phenylpyrimidine derivatives as new corrosion inhibitors for cold rolled steel in hydrochloric acid solution. Corros Sci 87:27–39

36. Khadraoui A, Khelifa A, Hadjmeliani M, Mehdaou R, Hachama K, Tidu A, Azari Z, Obot IB, Zarrouk A (2016) Extraction, characterization and anti-corrosion activity of *Mentha pulegium*

oil: weight loss, electrochemical, thermodynamic and surface studies. J Mol Liq 216:724–731

37. Anusuya N, Saranya J, Sounthari P, Zarrouk A, Chitra S (2017) Corrosion inhibition and adsorption behaviour of some bis-pyrimidine derivatives on mild steel in acidic medium. J Mol Liq 225:406–417

38. Döner A, Solmaz R, Özcan M, Kardas G (2011) Experimental and theoretical studies of thiazoles as corrosion inhibitors for mild steel in sulphuric acid solution. Corros Sci 53:2902–2913

39. Bentiss F, Lebrini M, Vezin H, Chai F, Traisnel M, Lagrené M (2009) Enhanced corrosion resistance of carbon steel in normal sulfuric acid medium by some macrocyclic polyether compounds containing a 1,3,4-thiadiazole moiety: AC impedance and computational studies. Corros Sci 51:2165–2173

40. Boucherit L, Douadi T, Chafai N, Al-Noaimi M, Chafaa S (2018) The inhibition activity of 1,10–bis(2-formylphenyl)-1,4,7,10–tetraoxadecane (Ald) and its schiff base (L) on the corrosion of carbon steel in HCl: experimental and theoretical studies. Int J Electrochem Sci 13:3997–4025

41. Fiala A, Boukhedena W, Lemallem SE, Ladouani HB, Allal H (2019) Inhibition of carbon steel corrosion in HCl and H_2SO_4 solutions by ethyl 2-cyano-2-(1,3-dithian-2-ylidene) acetate. J Bio Tribo Corros 5:42. https://doi.org/10.1007/s40735-019-0237-5

42. Saranya J, Benhiba F, Anusuya N, Subbiah R, Zarrouk A, Chitra S (2020) Experimental and computational approaches on the pyran derivatives for acid corrosion. Colloids Surf A 603:125231

43. El Ouadi Y, Abrigach F, Bouyanzer A, Touzani R, Riant O, ElMahi B, El Assyry A, Radi S, Zarrouk A, Hammouti B (2015) Corrosion inhibition of mild steel by new N-heterocyclic compound in 1 M HCl: experimental and computational study. Der Pharma Chem 7(8):265–275

44. Mashuga ME, Olasunkanmi LO, Verma C, Sherif ESM, Ebenso EE (2020) Experimental and computational mediated illustration of effect of different substituents on adsorption tendency of phthalazinone derivatives on mild steel surface in acidic medium. J Mol Liq 305:112844

45. Boutouil A, Laamari MR, Elazhary I, Bahsis L, Anane H, Stiriba SE (2020) Towards a deeper understanding of the inhibition mechanism of a new 1,2,3-triazole derivative for mild steel corrosion in the hydrochloric acid solution using coupled experimental and theoretical methods. Mater Chem Phys 241:122420

46. El Faydy M, Galai M, EbnTouhami M, Obot IB, Lakhrissi B, Zarrouk A (2017) Anticorrosion potential of some 5-amino-8-hydroxyquinolines derivatives on carbon steel in hydrochloric acid solution: gravimetric, electrochemical, surface morphological, UV–visible, DFT and Monte Carlo simulations. J Mol Liq 248:1014–1027

47. Khattabi M, Benhiba F, Tabti S, Djedouani A, El Assyry A, Touzani R, Warad I, Oudda H, Zarrouk A (2019) Performance and computational studies of two soluble pyran derivatives as corrosion inhibitors for mild steel in HCl. J Mol Struct 1196:231–244

48. Shaban SM (2016) N-(3-(dimethyl benzyl ammonio) propyl) alkanamide chloride derivatives as corrosion inhibitors for mild steel in 1M HCl solution: experimental and theoretical investigation. RSC Adv 6:39784–39800

49. Shaban SM, Aiad I, El-Sukkary MM, Soliman EA, El-Awady MY (2015) Inhibition of mild steel corrosion in acidic medium by vanillin cationic surfactants. J Mol Liq 203:20–28

50. Kumar R, Yadav OS, Singh G (2017) Electrochemical and surface characterization of a new ecofriendly corrosion inhibitor for mild steel in acidic media: a cumulative study. J Mol Liq 237:413–427

51. Díaz-Cardenas MY, Valladares-Cisneros MG, Lagunas-Rivera S, Salinas-Bravo VM, Lopez-Sesenes R, Gonzalez-Rodríguez JG (2017) Peumusboldus extract as corrosion inhibitor for carbon steel in 0.5 M sulfuric acid. Green Chem Lett Rev 10(4):257–268

52. Zarrouk A, Hammouti B, Al-Deyab SS, Salghi R, Zarrok H, Jama C, Bentiss F (2012) Corrosion inhibition performance of 3,5-diamino-1,2,4-triazole for protection of copper in nitric acid solution. Int J Electrochem Sci 7:5997–6601

53. Zarrok H, Zarrouk A, Salghi R, Oudda H, Hammouti B, Ebn Touhami M, Bouachrine M, Boukhris S (2012) A combined experimental and theoretical study on the corrosion inhibition and adsorption behaviour of quinoxaline derivative during carbon steel corrosion in hydrochloric acid. Port Electrochim Acta 30(6):405–417

54. Rajendraprasad S, Ali S, Prasanna BM (2020) Electrochemical behavior of N[1]-(3-methylphenyl)piperidine-1,4-dicarboxamide as a corrosion inhibitor for soft-cast steel carbon steel in 1 M HCl. J Fail Anal Preven 20:235–241

55. Zarrok H, Salghi R, Zarrouk A, Hammouti B, Oudda H, Bazzi Lh, Bammou L, Al-Deyab SS (2012) Investigation of the inhibition effect of N-1-naphthylethylenediamine dihydrochloride monomethanolate on the C38 steel corrosion in 0.5M H2SO4. Der Pharma Chem 4(1):407–416

56. Singh A, Ansari KR, Kumar A, Liu W, Songsong C, Lin Y (2017) Electrochemical, surface and quantum chemical studies of novel imidazole derivatives as corrosion inhibitors for J55 steel in sweet corrosive environment. J Alloys Compd 712:121–133

57. Kharbach Y, Qachchachi FZ, Haoudi A, Tourabi M, Zarrouk A, Jama C, Olasunkanmi LO, Ebenso EE, Bentiss F (2017) Anticorrosion performance of three newly synthesized isatin derivatives on carbon steel in hydrochloric acid pickling environment: electrochemical, surface and theoretical studies. J Mol Liq 246:302–316

58. Salhi A, Tighadouini S, El-Massaoudi M, Elbelghiti M, Bouyanzer A, Radi S, El Barkany S, Bentiss F, Zarrouk A (2017) Ketoenol heterocycles as new compounds of corrosion inhibitors for carbon steel in 1 M HCl: weight loss, electrochemical and quantum chemical investigation. J Mol Liq 248:340–349

59. Solomon MM, Umoren SA (2016) In-situ preparation, characterization and anticorrosion property of polypropylene glycol/silver nanoparticles composite for mild steel corrosion in acid solution. J Colloid Interface Sci 462:29–41

60. Prabakarana M, Kima SH, Oha YT, Rajb V, Chung IM (2017) Anticorrosion properties of momilactone a isolated from rice hulls. J Ind Eng Chem 45:380–386

61. Saxena A, Prasad D, Haldhar R (2018) Use of Asparagus racemosus extract as green corrosion inhibitor for mild steel in 0.5 M H2SO4. J Mater Sci 53:8523–8535

62. Rbaa M, Fardioui M, Verma C, Abousalem AS, Galai M, Ebenso EE, Guedira T, Lakhrissi B, Warad I, Zarrouk A (2020) 8-Hydroxyquinoline based chitosan derived carbohydrate polymer as biodegradable and sustainable acid corrosion inhibitor for mild steel: experimental and computational analyses. Int J Biol Macromol 155:645–655

63. Cao S, Liu D, Zhang P, Yang L, Yang P, Lu H, Gui J (2017) Green Brönsted acid ionic liquids as novel corrosion inhibitors for carbon steel in acidic medium. Sci Rep 7:8773. https://doi.org/10.1038/s41598-017-07925-y

64. El Yaktini A, Lachiri A, El Faydy M, Benhiba F, Zarrok H, El Azzouzi M, Zertoubi M, Azzi M, Lakhrissi B, Zarrouk A (2018) Practical and theoretical study on the inhibitory inflences of new azomethine derivatives containing 8-hydroxyquinoline moiety for the corrosion of carbon steel in 1 M HCl. Orient J Chem 34(6):3016–3029

65. Cherrak K, Benhiba F, Sebbar NK, Essassi EM, Taleb M, Zarrouk A, Dafali A (2019) Corrosion inhibition of mild steel by new benzothiazine derivative in a hydrochloric acid solution: experimental evaluation and theoretical calculations. Chem Data Collect 22:100252

66. Rouifi Z, Benhiba F, El Faydy M, Laabaissi T, About H, Oudda H, Warad I, Guenbour A, Lakhrissi B, Zarrouk A (2019) Performance and computational studies of new soluble triazole as corrosion inhibitor for carbon steel in HCl. Chem Data Collect 22:100242

67. Benhiba F, Benzekri Z, Guenbour A, Tabyaoui M, Bellaouchou A, Boukhris S, Oudda H, Warad I, Zarrouk A (2020) Combined electronic/atomic level computational, surface (SEM/EDS), chemical and electrochemical studies of the mild steel surface by quinoxalines derivatives anti-corrosion properties in 1 mol. L-1 HCl solution. Chin J Chem Eng 28(5):1436–1458

68. Saha SK, Ghosh P, Hens A, Murmu NC, Banerjee P (2015) Density functional theory and molecular dynamics simulation study on corrosion inhibition performance of mild steel by mercaptoquinoline Schiff base corrosion inhibitor. Phys E 66:332–341

69. Rbaa M, Benhiba F, Dohare P, Lakhrissi L, Touir R, Lakhrissi B, Zarrouk A, Lakhrissi Y (2020) Synthesis of new epoxy glucose derivatives as a non-toxic corrosion inhibitors for carbon steel in molar HCl: experimental, DFT and MD simulation. Chem Data Collect 27:100394

70. Rahmani H, Alaoui KI, El Azzouzi M, Benhiba F, El Hallaoui A, Rais Z, Taleb M, Saady A, Labriti B, Aouniti A, Zarrouk A (2019) Corrosion assessement of mild steel in acid environment using novel triazole derivative as a anti-corrosion agent: a combined experimental and quantum chemical study. Chem Data Collect 24:100302

71. Olasunkanmi LO, Obot IB, Ebenso EE (2016) Adsorption and corrosion inhibition properties of N-{n-[1-R-5-(quinoxalin-6-yl)-4, 5-dihydropyrazol-3-yl] phenyl} methanesulfonamides on mild steel in 1 M HCl: experimental and theoretical studies. RSC Adv 6:86782–86797

72. Benhiba F, Hsissou R, Benzekri Z, Belghiti ME, Lamhamdi A, Bellaouchou A, Guenbour A, Boukhris S, Oudda H, Warad I, Zarrouk A (2020) Nitro substituent effect on the electronic behavior and inhibitory performance of two quinoxaline derivatives in relation to the corrosion of mild steel in 1 M HCl. J Mol Liq 312:113367